Stability and rheological characterization of colloidal gas aphrons: influence of xanthan gum and sodium dodecyl sulfate

Magzhan Zhumabek, Aziza Kachkinova, Maxime Cochennec, Stéfan Colombano, Yerlan Amanbek, Yanwei Wang, Sagyn Omirbekov

Discover Applied Sciences

Research

Stability and rheological characterization of colloidal gas aphrons: influence of xanthan gum and sodium dodecyl sulfate

Magzhan Zhumabek[1] · Aziza Kachkinova[1] · Maxime Cochennec[4] · Stéfan Colombano[4] · Yerlan Amanbek[3] · Yanwei Wang[1,2] · Sagyn Omirbekov[1]

Received: 26 December 2024 / Accepted: 4 April 2025
Published online: 02 May 2025

Abstract
This study explores the stability and rheological properties of colloidal gas aphrons (CGAs) prepared with varying concentrations of xanthan gum (XG) and sodium dodecyl sulfate (SDS). Static stability was assessed by monitoring CGA volume changes over time in a graduated cylinder, while dynamic flow behavior was analyzed using a rotational rheometer to measure yield stress and viscosity at different shear rates. Rheological models were employed to characterize CGA behavior. The results showed that increasing the concentrations of XG and SDS enhanced the structural stability and viscoelastic properties of CGAs. The CGAs exhibited non-Newtonian fluid behavior, which the Herschel-Bulkley-Papanastasiou model accurately described. Yield stress and viscosity increased with higher XG concentrations, demonstrating the system's ability to maintain high viscosity at low shear rates while exhibiting shear-thinning behavior at higher shear rates. An optimal combination of XG and SDS concentrations was identified, which improved CGA stability, prolonged liquid retention, and minimized bubble coalescence. These findings provide important insights into how CGAs remain stable and flow. This knowledge will help in using CGAs in different industries and environmental processes.

Article Highlights

- Detailed rheological analysis of colloidal gas aphrons (CGAs) using shear, amplitude, and frequency sweep tests.
- Optimized XG-SDS formulations enhance foamability and CGA stability.
- The Herschel-Bulkley-Papanastasiou model accurately describes the shear-dependent viscosity of CGAs ($R^2 > 0.999$).

Keywords Colloidal gas aphrons · Xanthan gum · Microfoam · Rheology · Stability · Yield stress · Foamability · Biopolymer

Supplementary Information The online version contains supplementary material available at https://doi.org/10.1007/s42452-025-06884-8.

✉ Sagyn Omirbekov, sagyn.omirbekov@nu.edu.kz | [1]Center for Energy and Advanced Materials Science, National Laboratory Astana, Nazarbayev University, Astana 010000, Kazakhstan. [2]Department of Chemical and Materials Engineering, School of Engineering and Digital Sciences, Nazarbayev University, Astana 010000, Kazakhstan. [3]Department of Mathematics, School of Sciences and Humanities, Nazarbayev University, Astana 010000, Kazakhstan. [4]BRGM, Orléans F-45060, France.

1 Introduction

Colloidal gas aphrons (CGAs) have gained interest for their unique structure. Initially described by Sebba [1], CGAs, also called microfoams, exhibit remarkable advantages over conventional foams [2], including reduced size and enhanced stability, which minimize pressure gradients during use [3]. CGAs exhibit immense potential and a broad spectrum of applications across various fields. These include environmental remediation (e.g., mobilizing pollutants in soil and groundwater)[4], wastewater treatment (removal of hydrophobic contaminants)[5], enhanced oil recovery (improved displacement of oil within reservoirs) [6], drilling fluids (loss prevention and lubrication) [7], and even agriculture (efficient delivery of pesticides and fertilizers) [8]. The stability of CGAs is a critical factor influencing their suitability for diverse applications. CGAs are intricate systems comprising a gas phase encapsulated within an aqueous solution, typically stabilized using surfactants and polymers. Surfactants play a pivotal role by reducing surface tension during aphron formation and creating multilayered bubble walls that establish a stable network structure [9].

One of CGA's key components is surfactants, categorized as ionic (cationic and anionic) or nonionic [10–12]. It has been shown that CGA stability is achieved through the interplay of surface tension and liquid film properties that prevent bubble collapse [5]. The double-layer arrangement of surfactant molecules, with hydrophobic segments oriented inward and hydrophilic parts facing outward, enhances mechanical stability and inhibits coalescence. Studies [11, 13] have highlighted that ionic surfactants, such as sodium dodecyl sulfate (SDS), outperform nonionic surfactants in stabilizing aphrons due to stronger intermolecular forces in the bubble film. Experimental evaluations [14] have demonstrated that the stability and size of CGAs improve with longer alkyl chain lengths in surfactants, attributed to enhanced hydrophobic interactions. Polymers such as xanthan gum (XG) are often used as stabilizers, increasing solution viscosity, reducing bubble size, and improving liquid retention. For instance, Nareh'ei et al. [15] found that CGAs achieved optimal stability at an XG concentration of approximately 6420 ppm, supported by rheological analysis using various models, including Bingham Plastic and Power Law. In related studies [16, 17], adding XG and SDS to CGAs significantly enhanced stability by reducing liquid drainage and maintaining bubble structure over extended periods. These findings suggest that XG forms a protective layer around the bubbles, reducing the likelihood of coalescence, while SDS further contributes to stability through its surfactant properties.

Despite advancements in understanding CGA properties, gaps remain in analyzing their interactions under varying polymer and surfactant concentrations and their behavior under mechanical stresses. Existing studies [18–20] have primarily focused on the shear-thinning behavior, yield stress, and the effect of weighting agents on polymer solutions without fully exploring the long-term stability or viscoelastic properties of CGAs under dynamic conditions.

This study addresses these gaps by comprehensively evaluating CGA stability and rheological behavior across various XG and SDS concentrations. Systematic analyses of CGA foaming behavior, viscoelastic characteristics, and viscosity degradation over time are presented for the first time. Amplitude and frequency sweep tests are employed to assess the elastic and viscous properties of CGAs, offering new insights into the mechanisms driving their stability. Using Cole–Cole diagrams provides enhanced insights into the balance between viscous and elastic contributions, which helps optimize CGA formulations for improved performance under challenging operational conditions. By integrating advanced rheological techniques and detailed compositional analyses, this research provides valuable data for designing CGAs with superior stability, prolonged liquid retention, and improved environmental compatibility.

The manuscript is organized as follows: Sect. 1: The Introduction reviews CGAs, their significance, and existing research gaps. Section 2: Materials and Methods detail the experimental setup, including CGA preparation, stability tests, and rheological experimental details. Section 3: Results and Discussion present findings on CGA stability, rheology, and model applications, highlighting industrial and environmental relevance. Section 4: Conclusions summarize key insights, emphasizing CGA stability, rheological behavior, and potential applications. Additional data and extended discussions are provided in the Supplementary Information.

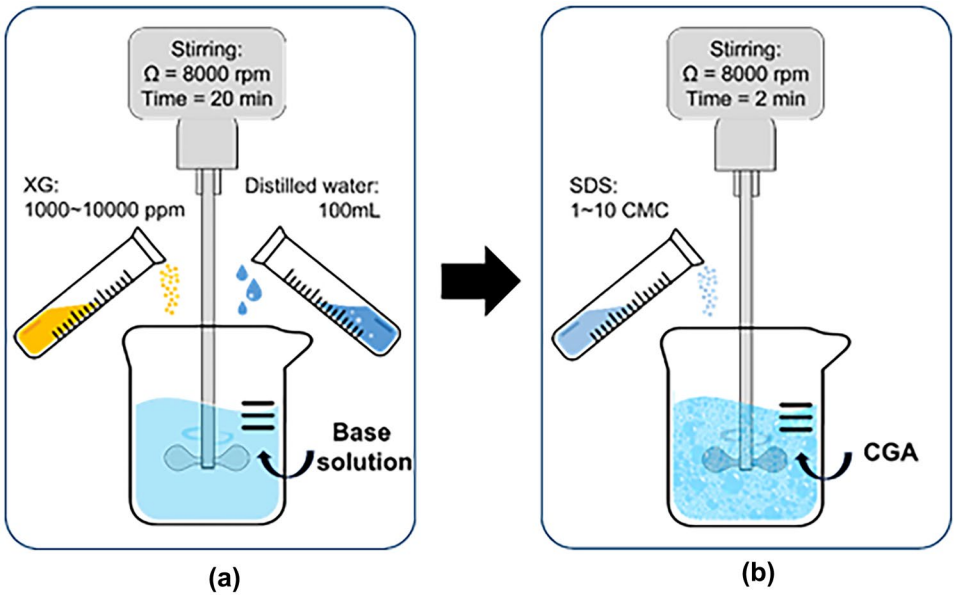

Fig. 1 Schematic representation of the CGA generation process: **a** Base solution preparation, **b** CGA formation

2 Materials and methods

In this study, various concentrations of xanthan gum (XG) were added as a thickening agent, while sodium dodecyl sulfate (SDS) was selected as the aphronatizing agent for the formation of colloidal gas aphrons (CGAs). The selection of these materials was guided by their environmental friendliness, market availability, and superior performance characteristics [21]. XG is a high-molecular-weight (≥ 1 million g/mol) extracellular polysaccharide produced by *Xanthomonas species* through bacterial fermentation [22]. It is widely used as a rheology modifier due to its high viscosity at low concentrations, shear-thinning behavior, and stability over a broad pH range. XG is a biodegradable, low-toxicity polymer that aligns with green chemistry and circular economy principles, making it particularly suitable for oxygen-limited environments [23, 24]. The XG polymer powders used in this study were supplied by Sigma-Aldrich (St. Louis, USA). SDS is an anionic surfactant that is biodegradable under aerobic conditions, with its degradation accelerated by adapted microbial communities. SDS efficiently reduces surface tension, improves foamability, and synergistically interacts with XG to stabilize CGAs, offering cost-effectiveness and performance advantages over alternatives like non-ionic or cationic surfactants. SDS is a white powder with 98.5% purity, limited adsorption on soil surfaces, and a critical micelle concentration (CMC) of 0.23 ± 0.01% (wt/mass), making it suitable for chemical and biological applications. Fisher Scientific International (Hampton, USA) provided the SDS used in this study. Moreover, as earlier studies [8, 25] demonstrated, the combination of XG and SDS significantly enhances CGA durability and rheological control.

A total of 36 CGA samples were prepared with varying concentrations of XG and SDS to evaluate their stability and rheological properties systematically. To ensure repeatability and statistical reliability, all experiments were conducted under controlled conditions. Freshly prepared CGAs were used in each trial to minimize variability due to aging or environmental factors. Each experiment was performed three times (n = 3), and the results were averaged to reduce random errors and improve measurement precision. The error bars in the graphs presented indicate the standard error of the mean (SEM) from these independent trials, providing a quantitative measure of the accuracy of the estimated mean. In many cases, the error bars may be smaller than the symbol size and not visible.

2.1 CGA generations

Preparation of base solution

Six different concentrations of XG polymer solutions, specifically 1000, 2000, 4000, 6000, 8000, and 10,000 ppm, were prepared to create CGA base solutions. Prior studies recommended the selected concentration ranges of 1000–10,000 ppm for XG [8, 25, 26] to achieve stable foam and optimum rheological control. We measured the required

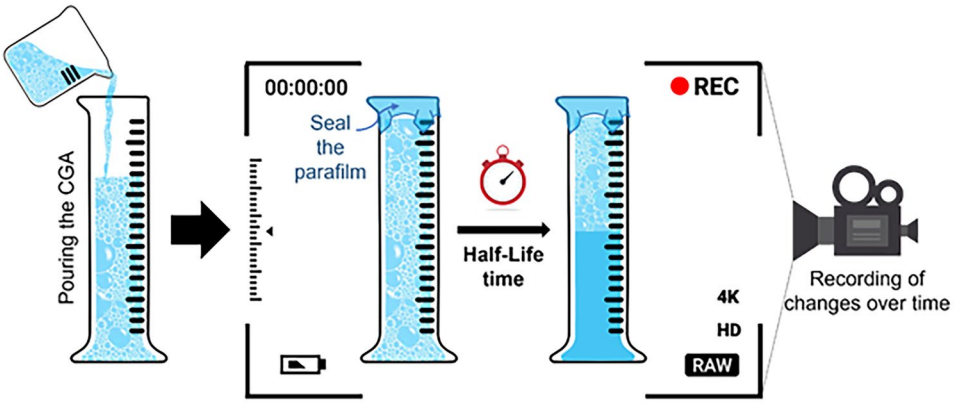

Fig. 2 Experimental setup for CGA stability experiment

amount of XG to be dissolved in 100 g of distilled water for each specified concentration. The solution was mixed thoroughly using a Silverson mixer for 20 min at 8000 rpm (see Fig. 1a).

CGA Generation

To generate CGA, we added six different concentrations of SDS surfactant solutions to each concentration of XG base solutions. The specific concentrations used were 1, 2, 4, 6, 8, and 10 CMC of SDS surfactant. The selected concentration ranges of 1–10 CMC for SDS were recommended in the study of Sebba [10], which shows that concentrations between 1 and 6 CMC are effective for microbubble stability. After weighing the components, we quickly added the SDS to the base solution. To verify that the surfactants were equally dispersed, we stirred the solution with a Silverson mixer at 8000 rpm for 2 min [15, 27, 28] (see Fig. 1b). Following this procedure, we determined the system's temperature and pH. Foamability was then determined by measuring the volume of CGA formed over the base solution, where the initial volume of the XG base solution was 100 mL (considered as 100%). After that, we tested the produced CGA for stability and rheological behavior.

2.2 Bulk CGA stability test

The stability of the base fluid for CGA can be considered to depend on its ability to resist changes in bubble size, bubble volume, and fluid distribution. Given that the densities of the aphrons and the base fluid are different, it can be observed that the bubbles tend to rise upwards, and the fluid settles downwards. We performed a series of static drainage experiments over time to gain insight into the homogeneity and stability of the CGA. The static experiments included measuring the drainage rate and monitoring the phase transition of CGA to liquid under static equilibrium conditions (Fig. 2). All experiments were conducted at atmospheric pressure, allowing us to evaluate the system's stability under standard conditions.

For static drainage tests, 100 mL of freshly prepared CGA-based solution was first poured into a graduated cylinder. The top was sealed with a parafilm for airtightness. With time, the total height (H_t) of the solution decreased. In addition, the CGA gradually turned into liquid, and drainage formed at the bottom of the cylinder. The half-life time was measured when 50 mL of microfoam was converted to a liquid phase [29]. The time when the microfoam completely collapsed was also measured. During the test, the height of the total liquid volume and the height of the drained volume were recorded.

2.3 Rheological test

An Anton Paar MCR 102e rheometer with a cone & plate geometry (1° degree and 50 mm diameter) was used to evaluate the rheological properties of CGA. This instrument allows a wide range of tests for detailed analysis of CGA behavior under different conditions. During all measurements, a constant room temperature (25 °C) corresponding to the conditions of actual CGA application was maintained, and the gap between the plates was set at 0.98 mm. Freshly prepared samples were used before each study to ensure the accuracy of the results. The rheometric studies included the four tests:

(1) Single shear rate test: calculation of viscosity at specific shear rates and stability over time. The tests were conducted at different shear rates: 0.1 s^{-1}, 1 s^{-1}, and 10 s^{-1} for 120 s [30, 31].

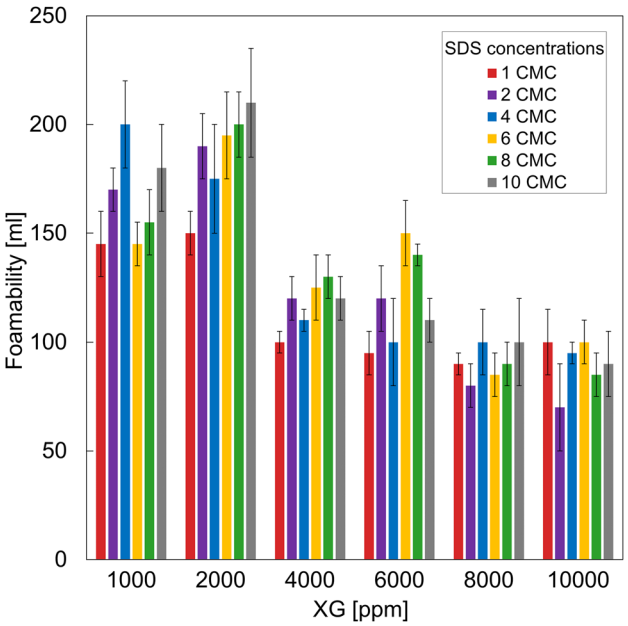

Fig. 3 Foamability of CGA as a function of XG concentration at varying SDS concentrations (expressed in multiples of the critical micelle concentration, CMC) ($t = 0$ min)

(2) Flow curve test: to construct the flow curve, the viscosity values of CGA were measured at gradually increasing and decreasing shear rates. Calculations were conducted gradually, increasing the shear rate from 0.1 to 100 s^{-1} The main objective was to determine of the yield stress of CGA [32–34].
(3) Amplitude sweep test: The amplitude shear test was conducted to evaluate the linear viscoelastic properties of CGA. The strain amplitude increased during the test, and the storage and loss modulus were recorded. The strain amplitude fluctuations occurred with a frequency of 1 Hz [32, 34].
(4) Frequency sweep test: in this experiment, the loss modulus (G″) and storage modulus (G′) are analyzed as a function of frequency in the linear viscoelastic domain. In frequency sweep tests, measurements are taken at a constant strain amplitude while the magnitude of the frequency is varied. This analysis is usually performed to describe the time behavior of the specimen over a non-destructive strain range. The oscillatory frequency sweep is performed in the 100–0.1 rad/s range at 0.4% constant strain amplitude [34, 35].

The flow curve experimental data were fitted by a continuous Herschel Bulkley-Papanastasiou (H-B-P) model, in which the shear viscosity (μ) is described as follows:

$$\mu(\dot{\gamma}) = K\dot{\gamma}^{n-1} + \frac{\tau_0}{\dot{\gamma}}[1 - \exp(-m\dot{\gamma})] \quad (1)$$

where τ (Pa) is the shear stress, $\dot{\gamma}$ (s^{-1}) is the shear rate, τ_0 (Pa) is the yield stress, K ($Pa.s^n$) is the consistency, m (s) controls the exponential growth of stress, which has dimensions of time and n (dimensionless) is the flow behavior index, respectively. Other empirical rheological models were also considered, and as documented in the Supporting Information, the H-B-P model obtained the best fit.

3 Results and discussions

3.1 Effect of XG and SDS concentrations on CGA stability

The study of foamability is essential for understanding CGA stability and the process involved in CGA formation. Fig. 3 presents the results of the foamability of CGA with respect to the XG and SDS concentrations across all 36 samples. The data presented allow us to analyze the effects of both XG and SDS concentrations on the foam ability of the system, highlighting the interaction between the polymer and surfactant and their combined effect on the foamability.

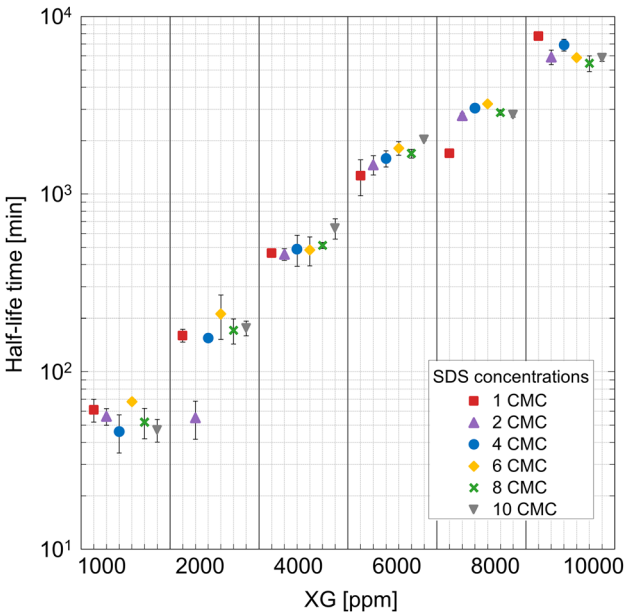

Fig. 4 CGA stability represented by half-life time plotted against XG concentration at varying SDS concentrations (expressed in multiples of CMC) for all 36 samples. Data are presented as mean ± SEM (n = 3), and note that the error bars may be smaller than the symbol size and therefore invisible

Foamability is determined by measuring the volume of CGA generated with the base polymer solution volume initially set to 100 mL (considered as 100%) before stirring.

The results indicate a general trend of decreasing foamability as the concentration of XG exceeds 2000 ppm. As shown in Fig. 3, two main aspects can be distinguished. The first is the effect of the polymer, and the second is the effect of the surfactant on the formation of CGA (foaming). At low XG concentrations (1000 and 2000 ppm), a relatively lower degree of molecular interaction is present in the solution, which favors the effective formation of an interfacial film around the bubbles, thus improving foaming. With increasing XG concentration (4000–10,000 ppm), structural changes in solution are observed due to increased intermolecular interactions between the polymer chains. This can lead to the formation of a denser mesh structure, which, on the one hand, contributes to the stabilization of already formed bubbles but, on the other hand, limits the penetration of air into the solution. This structure prevents the formation of new bubbles and their movement, which reduces foaming efficiency. The positive effect of SDS concentrations on foamability is also noticeable, especially at lower XG concentrations. As SDS concentration increases, foamability improves due to lower surface tension, allowing for stable bubble formation. Nonetheless, at greater XG concentrations, the thickening action of XG takes precedence, outweighing the surfactant's effects. The synergistic interaction between XG and SDS is evident at low XG concentrations (1000–2000 ppm) when an optimal balance between solution viscosity and surfactant surface activity favors improved foaming. However, when the XG concentration is increased, the excessive increase in viscosity leads to weakening the synergistic effect, reducing the system's response to changes in SDS concentration. This behavior is consistent with previous studies investigating the relationship between surfactant content and solution viscosity. Binks et al. [36] showed that increasing the concentration of SDS enhances foaming behavior by lowering surface tension and stabilizing microbubbles. An optimal SDS concentration of approximately 5 g/L yields CGA's highest volume and stability. Additionally, the viscosity of the solution, influenced by the XG content, is also crucial to the system's stability. Prior studies [16, 37] have shown that high-viscosity solutions slow liquid drainage, increasing CGA half-life and overall stability. The results indicate a delicate balance between polymer concentration, surfactant activity, and solution viscosity to optimize foaming. In addition, a trend with increasing XG concentration shows that large polymer concentrations are ineffective in CGA because the foamability of CGA decreases. This research establishes a basis for further discussions on CGA stability and offers insights into enhancing CGA formation through optimized formulations.

Figure 4 illustrates the stability of CGA as indicated by its half-life time, which is influenced by the XG and SDS concentrations. CGA stability notably enhanced by increasing the concentration of XG, reaching a peak at 10,000 ppm. This enhancement is primarily attributed to the increased viscosity of the continuous phase, which suppresses liquid drainage and delays bubble coalescence. As a well-known rheology modifier, XG is expected to increase the bulk and interfacial viscosity, which slows liquid drainage and helps maintain the structural integrity of the CGAs over time. The reduction in liquid drainage plays a crucial role in stabilizing CGAs, as slower drainage rates extend the half-life of the aphrons. Our findings are consistent with previous studies [38–41], demonstrating that higher XG concentrations improve CGA stability.

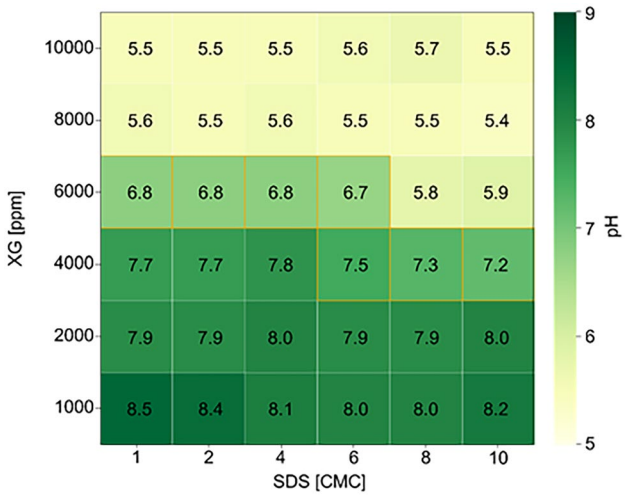

Fig. 5 pH profile of CGA solutions as a function of XG (Y-axis) and SDS (X-axis) concentrations. Numerical values indicate measured pH levels, and the neutral pH range (6.5–7.5) is highlighted

The effect of surfactants on the stability of CGA can also be seen in Fig. 4. In particular, the stability of CGA shows an increasing trend with increasing SDS concentration for solutions prepared at 4000, 6000, and 8000 ppm XG concentrations. However, we did not observe significant differences in solutions with 1000, 2000, and 10,000 ppm XG. This trend can be explained by the formation of SDS micelles after reaching a CMC, which then aggregate and interact with the polymer chains. This interaction was driven by several critical parameters, including enthalpy and free energy changes, which affect the stability and structure of the aggregates [42, 43]. Studies show that higher concentrations of SDS lead to an increase in solution viscosity, attributed to the formation of mixed micelles that act as cross-links between polymer chains [44, 45].

Among all the XG concentrations tested, 6000 ppm was identified as the optimum concentration, demonstrating excellent foamability and stability. Additionally, the interaction between XG and SDS creates a synergistic effect that enhances the CGA properties. The steric hindrance produced by XG, when combined with the surface activity of SDS, results in CGAs that are not only more stable but also exhibit improved foamability [39, 42–46].

3.2 pH test

Figure 5 presents the pH measurements for all 36 CGA formulations, illustrating the relationship between pH, XG concentration, and SDS concentration. A neutral pH range (6.5–7.5), indicative of optimal stability, is highlighted in orange. The results show that the pH remains within this neutral range at intermediate XG concentrations (4000–6000 ppm). However, deviations from neutrality are observed at both lower and higher XG concentrations, with the solution becoming more alkaline at low XG concentrations and more acidic at high XG concentrations. The influence of SDS on pH is most pronounced in the 4000–6000 ppm XG range, where increasing SDS concentration leads to a systematic pH reduction.

The results in Fig. 5 illustrate the relationship between pH and CGA content, which becomes more pronounced as the XG concentration increases. Higher XG concentrations correspond to lower pH values. Specifically, when the XG concentration is between 1000 and 4000 ppm, the system has an alkaline pH, while when the XG concentration increases from 6000 to 10,000 ppm, the pH of the solution starts to decrease, becoming more acidic. The effect of SDS is particularly noticeable at XG concentrations from 4000 to 6000 ppm, where the pH of the system decreases as the concentration of SDS increases.

Petkova et al. [47] showed that under low pH conditions, the system with SDS and polyvinyl amine (PVAm) exhibits more pronounced electrostatic interactions due to the polymer's increased charge density, which favors the system's stability. In this case, SDS, an anionic SDS, forms strong bonds with positively charged polymer molecules, reducing bubble drainage and coalescence [48, 49]. Confirming these findings, Sadahira et al. [49] observed that low pH favors the strength of the CGA structure by reducing the liquid drainage rate and increasing the bubble lifetime. These observations suggest that lower pH increases surface tension in surfactant systems, which in turn helps to prevent coalescence and improves the viscoelastic properties of the system [47].

At higher pH, a weakening of the interaction is observed, which leads to a decrease in the system's stability. These results are consistent with our observations for systems with XG and SDS, where the stability of CGA at low pH is maintained due to better interaction between the components.

Figure 5 also shows that at XG concentrations of 4000 ppm and 6000 ppm, the pH values remain stable in the neutral range (6.5–7.5), highlighted in orange. In contrast, at other concentrations, pH either exceeds 7.5 or falls below 6.5, indicating a possible disruption of the acid–base balance and a decrease in system stability. Thus, the 4000 ppm and 6000 ppm XG concentrations are most interesting for further studies as they provide pH stability within the neutral zone and are more promising for further analyses.

3.3 Rheological study

This section presents the results of rheological studies aimed at a detailed analysis of the stability of CGA under dynamic flow conditions. The behavior of the sample at different shear rates, as well as its viscoelastic characteristics, has been analyzed. The data obtained are consistent with a rheological model that can be used for further studies. The results provide essential information on CGA's rheological properties and overall behavior, contributing to better understand its dynamic characteristics.

3.3.1 Rheological stability of CGA: assessments at single shear rates

To evaluate the stability of CGA under flow conditions, single-shear rate tests were carried out at three different shear rates: 0.1 s^{-1}, 1 s^{-1}, and 10 s^{-1}. Figure 6 presents the time-dependent viscosity profiles obtained from these tests as follows: (a) for varying XG concentrations at a fixed SDS concentration of 6 CMC and (b) for varying SDS concentrations at a fixed XG concentration of 4000 ppm.

Figure 6a shows the effect of XG concentration on the solution viscosity at shear rates of 0.1 s^{-1}, 1 s^{-1}, and 10 s^{-1} at a fixed SDS concentration over 120 s. The stability of all CGAs for 120 s is observed. However, up to 10 s in the beginning, a viscosity increase is noticeable for all XG concentrations when the shear rate is 0.1 s^{-1}. This process is due to the alignment and stretching of polymer chains. Figure 6a also shows that the viscosity of the solution increases with increasing XG concentration. At concentrations of 8000 ppm and 10,000 ppm, a denser and more interconnected polymer network is formed, contributing to higher flow resistance. At the same time, the viscosity is much lower at low XG concentrations (e.g., 2000 ppm) due to weak inter-chain interaction and less developed network structure. XG's semi-rigid, rod-shaped molecular structure favors increased inter-chain interactions and, thus, viscosity as its concentration increases.

Figure 6b shows the effect of SDS concentration on the rheological characteristics of CGA systems at a fixed concentration of XG (4000 ppm). The results demonstrate that there is no pronounced dependence of viscosity on changes in SDS concentration. The viscosity coefficient remains almost constant at different SDS concentration and shear rates, indicating minimal effect of SDS content on the rheological properties of CGA over this range of conditions. The lack of a clear trend suggests that at a fixed XG concentration of 4000 ppm, the contribution of SDS to the overall viscosity of the system is minimal. Furthermore, data analysis over 120 s highlights the stability of systems based on XG, regardless of the SDS threshold.

This section of the study indicates that the viscosity of the solution increases with rising XG concentration across all tested shear rates. In contrast, the influence of SDS on viscosity within the CGA system appears insignificant. As demonstrated in Fig. 6, we intend to focus rheological studies on the effects of polymer concentrations. In our static studies, this SDS concentration has shown the most promising results in stabilizing the system and enhancing interface properties, leading us to fix the concentration at 6 CMC.

3.3.2 Rheological stability of CGA: assessments at flow curve test

The rheological properties of CGA systems with varying XG concentrations were evaluated by measuring the shear viscosity as a function of shear rate. Figure 7 shows rheological curves for systems containing a fixed SDS concentration of 6 CMC and varying concentrations of XG between 1000 and 10,000 ppm.

The results show a decreasing trend in viscosity with an increasing shear rate for all concentrations of XG. This shear-thinning behavior is more pronounced at higher XG concentrations. Additionally, the absolute viscosity values are significantly higher for CGA with increased XG concentration, particularly at low shear rates. At low shear rate of 0.1 s^{-1}, the viscosity increases by several orders of magnitude, from 0.45 Pa·s (1000 ppm XG) to 44 Pa·s (10,000 ppm XG). At

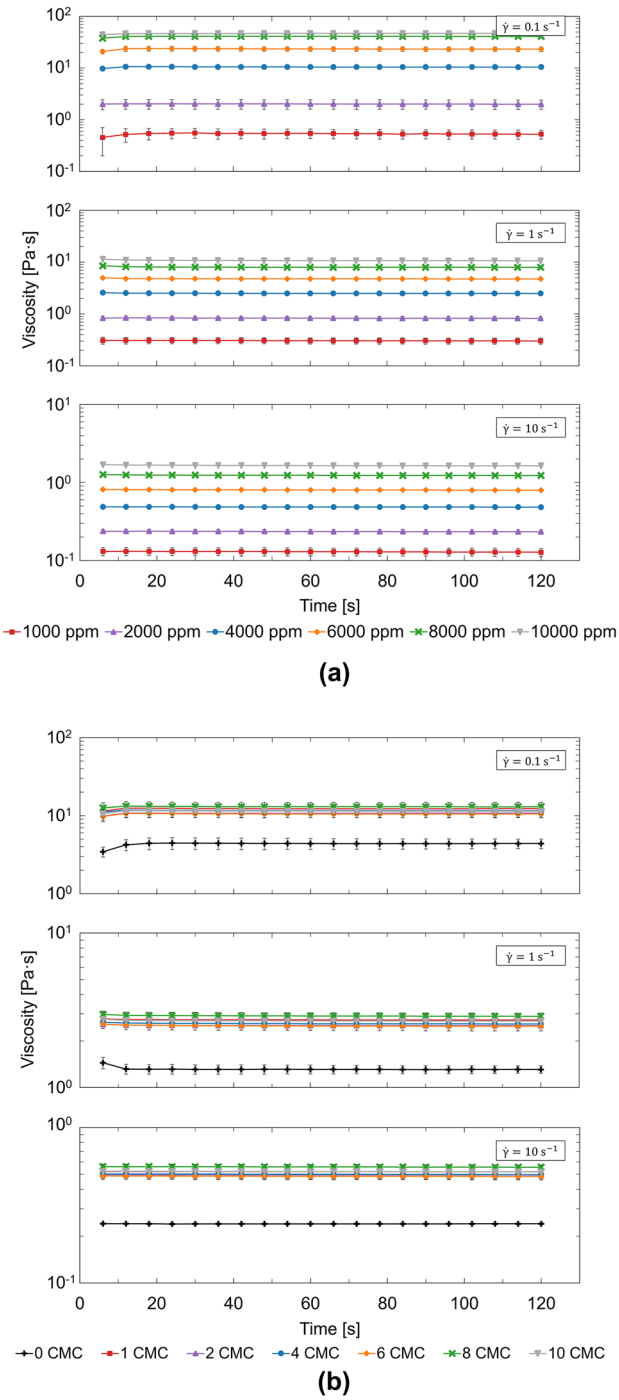

Fig. 6 Shear viscosity of CGAs at constant shear rates (0.1 s^{-1}, 1 s^{-1}, and 10 s^{-1}): **a** Effect of XG concentration at a fixed SDS concentration of 6 CMC; **b** Effect of SDS concentration at a fixed XG concentration of 4000 ppm. The data for 0 CMC correspond to an aqueous XG solution without SDS at a fixed XG concentration of 4000 ppm. Data are presented as mean ± SEM (n = 3). Note: error bars may be smaller than the size of the symbols and may not be visible

high shear rates (> 10 s^{-1}), the viscosity difference between CGA and different XG concentrations decreases due to the breakdown of the polymer structure and the transition to a less organized state.

The decrease in viscosity with increasing shear rate is characteristic of non-Newtonian fluids. This behavior occurs due to the alignment of polymer chains (XG molecules) in the flow direction, which minimizes intermolecular interactions and internal resistance to deformation. The enhanced network formation in the solution can explain the increase in viscosity with higher XG concentrations. At higher concentrations, XG molecules interact more extensively via hydrogen bonding and entanglement, increasing resistance to flow at low shear. This structural reinforcement contributes to higher initial viscosities. The fixed SDS concentration (6 CMC) ensures stable CGA generation, with SDS

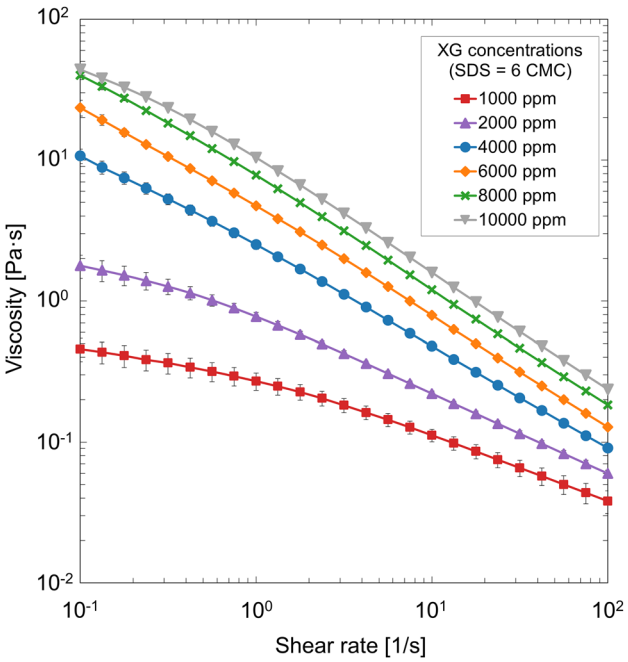

Fig. 7 Viscosity dependence of CGA on the shear rate at different XG concentrations and a fixed SDS concentration of 6 CMC. Data are presented as mean ± SEM (n = 3) and note that the error bars may be smaller than the symbol size and may therefore be invisible

acting as a surfactant to lower the surface tension and stabilize gas–liquid interfaces. However, the primary influence on viscosity stems from the XG, which governs the bulk rheological properties.

In Fig. 7, the initial values of shear stress before the viscosity reduction indicate the yield point for each concentration. The yield stress appears when the slope changes from horizontal (indicating solid-like behavior) to downward slope (fluid-like behavior). The yield stress increases with XG concentration, indicating a stronger network structure in the solution. For example, a solution with 8000–10000 ppm XG shows higher yield stress than those with 1000–4000 ppm. This trend is consistent with the understanding that higher XG concentrations lead to stronger intermolecular interactions, resulting in higher flow resistance at low shear rates.

At low shear rates, the viscosity of the solutions increases significantly with XG concentration. This trend is consistent with the results of García-Ochoa et al. [23], who attribute the high viscosity of XG solutions to the formation of an extensive network structure of polymer chains arising from hydrogen bonds and the intertwining of molecules. At high shear rates, the differences in viscosity between solutions with different XG concentrations decrease significantly, which is attributed to the transition of the polymer structure to a less ordered state. Choppe et al. [50] observed a similar behavior and noted that the XG molecules align with the flow direction under shear, decreasing intermolecular interactions and internal resistance.

In the study of Khan et al. [51], yield stress is an essential indicator of a material's ability to resist deformation before flow for the study of CGA rheology. They emphasized that increased yield stress is associated with increased structural organization and interactions within the system. These findings support our results for XG solutions, where higher XG concentrations lead to more pronounced intermolecular interactions such as hydrogen bonding and polymer chain entanglement. In particular, higher XG concentrations (e.g., 8000–10,000 ppm) show a significant increase in yield stress, indicating the formation of a strong network structure capable of resisting deformation at low shear rates. This structural enhancement in XG solutions is consistent with the mechanisms described by Khan et al. [51], where the yield stress increase is attributed to the ordering and strength of the material's internal structure.

Figure 8 shows the shear stress versus shear rate dependence for XG solutions with concentrations ranging from 1000 to 10,000 ppm at a fixed SDS concentration of 6 CMC. Experimental data, indicated by different symbols, were fitted with the H-B-P model (see Eq. 1), represented by dashed lines. The fitted parameters are tabulated in Table 1.

The shear stress increases with increasing shear rate for all XG concentrations, demonstrating a non-linear trend characteristic of shear-thinning fluids. The shear stress also increases with XG concentration, indicating that higher polymer content increases the resistance of the solution to shear deformation. For all XG concentrations at a fixed SDS level, shear liquefaction behavior can be observed, corresponding to lower flow resistance at higher shear rates. The increase in shear stress with shear rate and the nonlinear trend suggests a non-Newtonian fluid behavior dominated by shear thinning. This behavior arises due to the alignment of XG polymer chains in the flow direction, reducing intermolecular

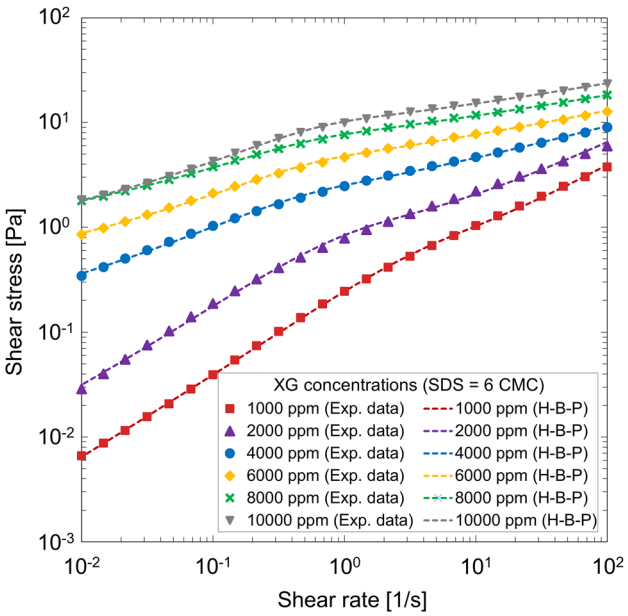

Fig. 8 Herschel-Bulkley-Papanastasiou (H-B-P) model fitting of flow curves (shear stress vs. shear rate) for different XG concentrations at a fixed SDS concentration. Symbols represent experimental data, while dashed lines indicate the model predictions

interactions and internal resistance. At higher XG concentrations, enhanced intermolecular entanglements and hydrogen bonding form a stronger structural network, which increases the shear stress at equivalent shear rates. The results in Fig. 8 can be correlated with data from the work of [52], which also investigates the shear stress-shear rate dependence for systems containing CGA. In this work, the authors show that such systems exhibit nonlinear rheological properties consistent with experimental data. In their study, they also observed that systems with different concentrations exhibit similar behavior—increasing concentration leads to an increase in initial yield stress and an increase in shear stress at low velocities. Still, at high velocities, the differences between concentrations flatten out [52].

The H-B-P model demonstrates high accuracy in fitting the experimental data, which confirms its applicability for modeling nonlinear rheological properties of the studied CGA. To evaluate the suitability of the rheological model for describing the viscoplastic properties of CGA, the average absolute relative error (AARE), root mean square error (RMSE), and coefficient of determination (R^2) were determined [19, 20]. The corresponding values for the H-B-P model are presented in Table 1. Also the table includes the Low-Shear Rate Viscosity (LSRV) values, measured at the shear rate of 0.01 s^{-1} (see Fig. 7).

With increasing XG concentration in the system, significant changes in the rheological characteristics were observed, indicating a progressive improvement in the solution's viscoelastic properties and structural stability. The yield stress (τ_0) increased about 20 times from 0.3291 Pa at 1000 ppm to 4.9248 Pa at 10,000 ppm, indicating the formation of a denser and stiffer polymer network requiring significant stress to break. The consistency coefficient (K) increased more than 28 times from 0.137 to 5.62 Pa s, indicating a substantial increase in the system's viscosity due to the high polymer concentration and its interactions with the solvent. At the same time, the flow index (n) decreased from 0.71 to 0.24, indicating the development of a pseudoplastic behavior in which the system becomes less flowable with increasing stress. This is due to the alignment of polymer chains under shear stress, which contributes to the thinning of the structure. The regularization parameter (m) increased from 0.39 to 3.36 at 8000 ppm of XG concentration before stabilizing at 2.79 at 10,000 ppm, demonstrating a smoother transition between linear and nonlinear strain regions at the initial stage and

Table 1 Fitting parameters of the Herschel-Bulkley-Papanastasiou (H-B-P) rheological model (Eq. 1) for CGAs: τ_0 (Pa) is the yield stress, K (Pa • s^n) is the flow consistency index, m (s) has dimensions of time, and n (dimensionless) is the flow behavior index

XG (ppm)	SDS (CMC)	τ_0	K	n	m	R^2	AARE	RMSE	LSRV (Pa • s)
1000	6	0.3291	0.137	0.71	0.39	0.9999	3.46%	0.0098	0.6489
2000	6	0.6081	0.608	0.60	1.54	0.9990	9.80%	0.0216	3.1562
4000	6	0.8728	1.664	0.35	3.66	0.9994	5.90%	0.0101	36.221
6000	6	1.8414	3.02	0.28	3.07	0.9995	5.24%	0.0079	87.685
8000	6	2.6650	5.15	0.24	3.36	0.9998	0.53%	0.0048	178.53
10,000	6	4.9248	5.62	0.26	2.79	0.9997	0.65%	0.0057	180.99

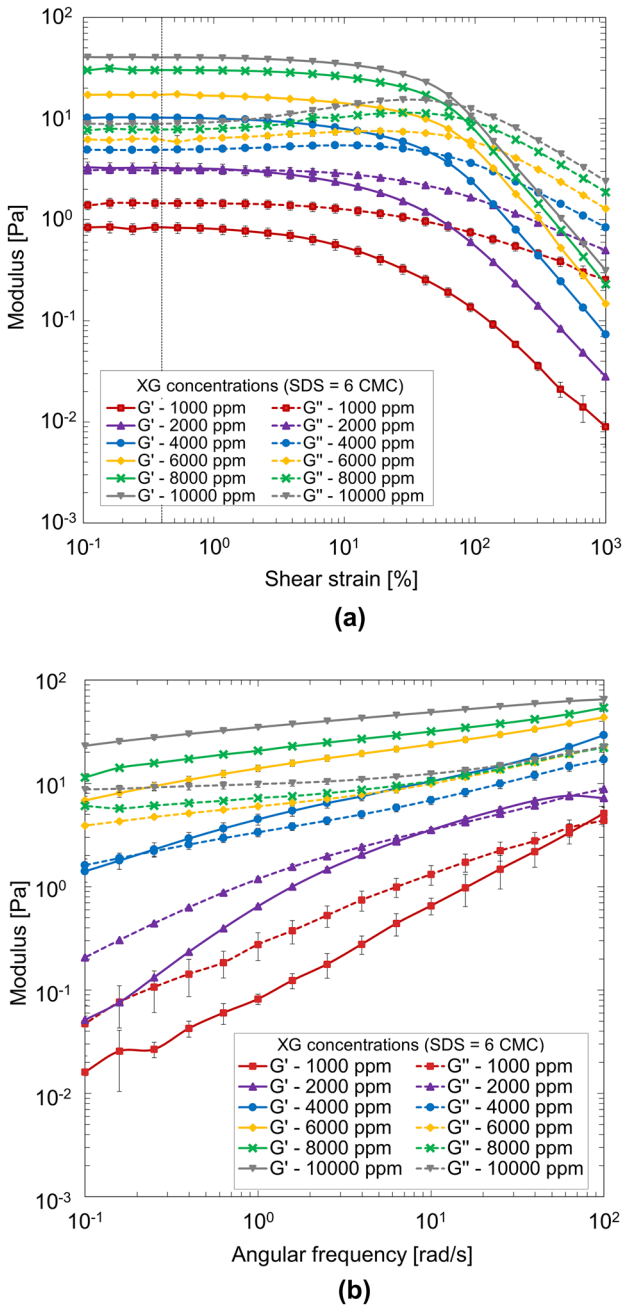

Fig. 9 Rheological behavior of CGAs demonstrating viscoelastic properties: **a** Variation of storage modulus (G′) and loss modulus (G″) as a function of strain amplitude from the amplitude sweep experiment, illustrating the linear viscoelastic region and the onset of structural breakdown. **b** Dependence of G′ and G″ on the angular frequency at a fixed shear strain of 1% obtained from frequency sweep measurements. Data are presented as mean ± SEM (n = 3), and the error bars may be smaller than the size of the symbols, which might render them invisible

increased structural stiffness at higher polymer concentrations. These changes confirm that increasing XG concentration significantly strengthens the solution structure, increasing its resistance to deformation and developing more complex rheological characteristics.

3.3.3 Rheological stability of CGA: assessments at amplitude sweep and angular frequency sweep test

Figure 9 shows the dynamic rheological analysis of XG with different concentrations (1000–10,000 ppm) and an SDS concentration of 6 CMC. Figure 9a presents the dependence of storage modulus (G′) and loss modulus (G″) on shear strain (%), which reflects the strain-dependent viscoelastic behavior of the CGA. Figure 9b shows the of G′ and G″ with angular frequency (rad/s), which demonstrates the frequency-dependent viscoelastic properties of the CGA. The solid lines characterize the G′ associated with the solution's elastic (solid-like) behavior. In contrast, the dashed lines show the

G″ reflecting the viscous (liquid-like) behavior. The different colored curves represent data for XG solutions with increasing concentrations, which allows us to analyze the effect of polymer concentration on the viscoelastic properties of the CGA.

In Fig. 9a, the storage modulus G′ decreases with increasing shear strain, indicating the manifestation of the shear thinning characteristic of polymer solutions. At low values of shear strain, G′ exceeds G″, indicating the dominance of solid-like (elastic) behavior of the CGA, except at a concentration of 1000 ppm. The loss modulus G″ also decreases with shear strain. Still, the decrease is less intense than that of G″ indicating a gradual transition of the system to a liquid-like (viscous) state. The modulus intersection points $G' = G''$, reflecting the balance between elastic and viscous properties, shifts toward higher strain values with increasing XG concentration, indicating an increase in the structural stability of the solution. The increase in G' and G'' values with increasing XG concentration suggests an increase in the viscoelasticity of the system due to the rise in the density of intermolecular interactions and the formation of a stronger polymer network.

In the plateau regime, when G' and G'' are stable, several research groups have studied the effect of strain amplitude [53–56]. The storage and loss modulus remains relatively constant when the strain is below a specific value, decreasing with increasing fluid fraction. This regime is known as the linear viscoelastic (LVE) regime. The LVE region was determined using amplitude sweep tests and was found to extend from 0.1 to 0.4% strain across all concentrations. For the frequency sweep experiments, a strain amplitude of 0.4% was selected based on strain sweep experiments, ensuring that the measurements remained within the LVE region. This ensures that the mechanical spectra presented in Fig. 9b represent the material's behavior in the linear viscoelastic regime. In the LVE region(0.1 to 0.4% strain), both G' and G'' remain constant [54], indicating that the molecular structure of CGA remains intact at small strains. This region is essential for the formulation stability of CGA in various applications, and it must withstand small mechanical stress (e.g., shaking or stirring) while maintaining its structure.

As the strain exceeds the LVE region (>0.5%), both moduli start to decrease, signaling the onset of non-linear viscoelastic behavior. This behavior has been observed in studies by [54, 57]. This decrease is due to the gradual breakdown of the XG network, with yield strain from 10% for all samples. The material transitions from a predominantly elastic (solid-like) response to a more viscous (liquid-like) response, characteristic of shear-thinning materials. Notably, G' decreases faster than G'' as strain increases, indicating a more significant weakening of elastic properties compared to viscous properties [54, 57–59]. This behavior is characteristic of XG's ability to flow under increased stress. XG concentration significantly affect the rheological properties. Higher concentrations (6000–10000 ppm) lead to higher G' and G'' values, showing increased resistance to deformation.

In Fig. 9b, the storage modulus G' consistently increases with increasing angular frequency for all concentrations studied, indicating an increase in the elastic properties of the system at high frequencies. Higher concentrations of XG lead to a significant increase in G' values over the entire frequency range, reflecting the strengthening of the elastic component of the material. The loss modulus G'' also increases with angular frequency. Still, its rate of increase is less than that of G'. The increase in both modulus G' and G'' with increasing XG concentration is associated with an increase in the degree of polymer chain entanglement and their interaction with SDS micelles, which contributes to the formation of a stronger viscoelastic network.

Frequency sweep tests complement amplitude sweep by providing information on how the storage and loss modulus varies with angular frequency. Moreover, the ratio between G' and G'' in frequency sweep can show the structural integrity of the material and the presence of interactions between colloidal particles [59, 60]. At 1000 ppm G'' exceeds G' at all angular frequencies, indicating the dominance of the viscous component and the weakness of the polymer network. This behavior is characteristic of the liquid-like system. At 2000 ppm at low frequencies G'' also exceeds G' at low frequencies, but with increasing frequency G' approaches G'', indicating the initial formation of a weak structural network and a transient behavior between liquid-like and solid-like states. This result implies that the polymer network is not sufficiently developed to form a structured matrix at low XG concentration. The structure at low XG, CGA concentrations is unstable and organized enough to exhibit significant elastic strength.

For samples with 4000 ppm concentration, especially at low frequencies, G'' is initially higher than G', which means that these solutions exhibit viscosity-dominated behavior in this region [60, 61]. This suggests that at low frequencies, the 4000 ppm solutions dissipate more energy in the form of viscosity, i.e., they behave more like liquids. With increasing frequency, G' exceeds G'', reflecting the transition to elastic behavior characteristic of a more solid response [62]. At higher XG concentrations (6000–10000 ppm), the values of G' and G'' shift upwards ($G' > G''$), showing higher strain stability (higher G') and higher energy dissipation (higher G''). This indicates that these solutions exhibit predominantly elastic-dominated behavior even at low strain rates. This elasticity helps maintain the material underload's structural integrity, making XG useful in applications requiring both stability and deformability.

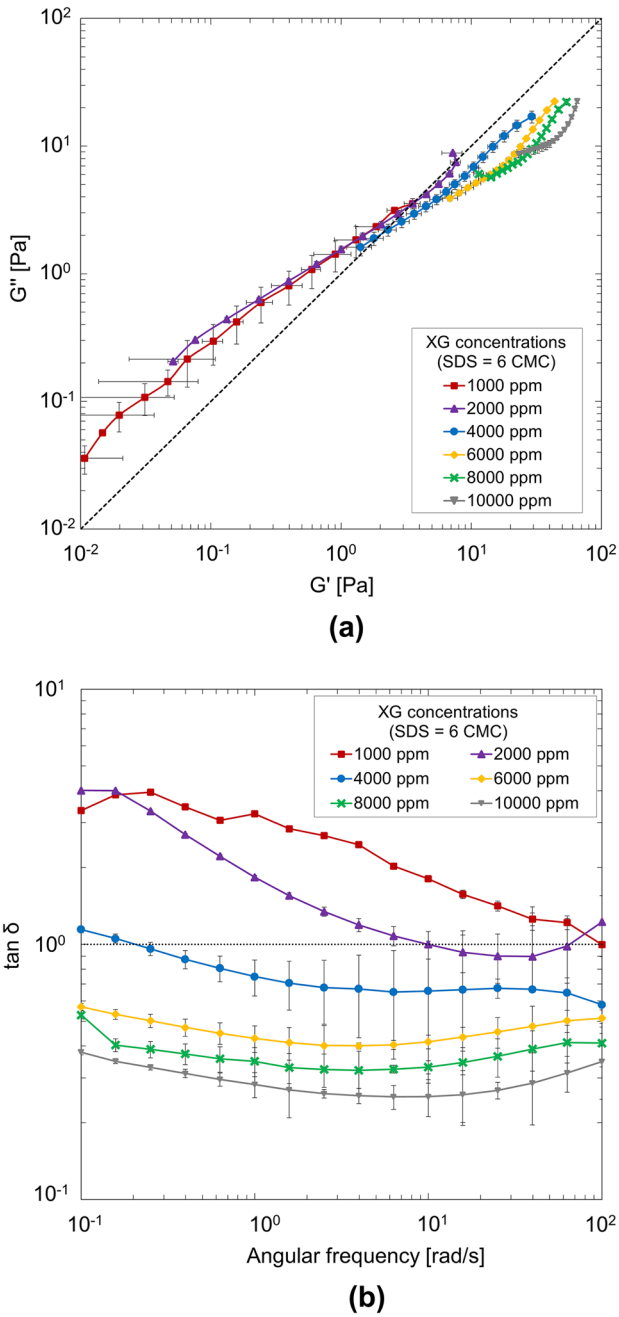

Fig. 10 **a** Cole–Cole plot of CGAs: Loss modulus (G'') versus storage modulus ($G\prime$) for different XG concentrations; **b** Tangent delta ($\tan\delta = G''/G\prime$) versus angular frequency for CGAs with different XG concentrations. The SDS concentration is fixed at 6 CMC. Data are presented as mean ± SEM (n = 3), and the error bars may be smaller than the size of the symbols, which might render them invisible

The Cole–Cole plot is a graphical representation where loss modulus (G'') is plotted against the storage modulus ($G\prime$) to assess the viscoelastic properties of a material. The Cole–Cole plot of CGAs shown in Fig. 10a reveals a shift in viscoelastic behavior with increasing XG concentration. At low modulus values, CGAs with 1000 and 2000 ppm XG exhibit $G'' > G'$, with data points lying above the 45° line, indicating a more viscous-dominated response. As XG concentration increases, the data trend closer to the 45° line, suggesting more balanced viscoelastic behavior. At high modulus values, the results for 1000 ppm and 2000 ppm XG align closer to the 45° line, whereas higher XG concentrations show a clear trend below the line, with slopes less than 1, indicating an increasingly elastic-dominated behavior. These findings demonstrate that XG concentration influences the relative contributions of elastic and viscous properties in CGAs and higher XG concentrations enhance the elasticity of CGAs, which could also be relevant for their stability and performance under shear.

The tangent delta ($\tan\delta = G''/G'$) versus angular frequency plot (see Fig. 10b) demonstrates a consistent decrease in $\tan\delta$ with increasing angular frequency across all samples, indicating a transition toward a more elastic-dominated response at higher frequencies. For high XG concentrations (6000 ppm, 8000 ppm, and 10,000 ppm), $\tan\delta$ remains below

1 over the entire frequency range $(10^{-2}$ to 10^{2} rad/s$)$, confirming that the storage modulus exceeds the loss modulus, meaning elastic behavior dominates across all measured frequencies. This trend suggests that increasing XG concentration enhances the elastic contribution to CGA rheology, leading to greater resistance to deformation under oscillatory shear.

4 Conclusion

In this study, we have systematically explored the intricate relationship between the stability, rheology, and foamability of CGAs prepared using XG and SDS. The findings provide a comprehensive understanding of how polymer and surfactant concentrations influence the behavior of CGAs, offering valuable insights for optimizing their formulation in various industrial applications.

- The results demonstrate that XG and SDS concentrations play a pivotal role in determining the stability and rheological properties of CGAs. Intermediate concentrations of XG (4000–6000 ppm) and SDS (4–6 CMC) were found to offer an optimal balance between foamability and stability. Higher XG concentrations, while enhancing stability, led to reduced foamability due to increased viscosity, which hindered bubble formation. Conversely, lower XG concentrations facilitated better foamability but at the cost of reduced stability. The synergistic effect of XG and SDS was particularly evident at intermediate concentrations, where the combination of increased viscosity from XG and reduced surface tension from SDS resulted in highly stable CGAs with desirable rheological properties.
- The rheological analysis revealed that CGAs exhibit pseudoplastic behavior, with viscosity decreasing as the shear rate increases. This shear-thinning characteristic is critical for applications requiring flow under stress, such as in enhanced oil recovery or wastewater treatment. The H-B-P model effectively described the rheological behavior of CGAs, achieving high accuracy ($R^2 > 0.999$) across all tested concentrations. The model parameters, including yield stress (τ_0) and coefficient consistency (K), highlighted the strengthening of the viscoelastic network with increasing XG concentration, further emphasizing the importance of polymer concentration in controlling CGA stability.
- Dynamic rheological tests, including amplitude and frequency sweeps, provided deeper insights into the viscoelastic properties of CGAs. The transition from viscous to elastic behavior with increasing angular frequency underscored the formation of a structured network at higher XG concentrations. This network, reinforced by the interaction between XG and SDS, enhances the structural integrity of CGAs, making them suitable for applications requiring both stability and deformability.

From a practical perspective, the findings of this study have significant implications for the design and optimization of CGA-based technologies. The ability to fine-tune the concentrations of XG and SDS allows for the customization of CGAs to meet specific application requirements, whether in environmental remediation, drug delivery, or enhanced oil recovery. Moreover, the use of environmentally friendly and cost-effective materials like XG and SDS aligns with global sustainability trends, making CGAs a viable option for large-scale industrial applications.

Although this study provides a solid foundation for understanding the behavior of CGA, further research is needed. Future studies should systematically investigate the effects of additional variables, such as pressure changes and extreme environmental conditions (e.g., high salinity or acidic/alkaline environments), on the stability and effectiveness of CGA. These factors are critical for applications such as enhanced oil recovery and soil remediation. The behavior of CGAs in porous media must be studied to evaluate their transport properties, retention and long-term stability. This is particularly relevant for applications such as groundwater remediation and oil displacement in reservoirs. There is a need to evaluate the stability and performance of CGAs when interacting with light non-aqueous phase liquids (LNAPLs) such as petroleum-based contaminants. This study may provide insight into the optimization of CGA for environmental cleanup applications.

This work not only advances our understanding of the stability and rheology of CGAs but also highlights the potential of XG and SDS as key components in the development of sustainable and efficient CGA formulations. By bridging the gap between fundamental research and practical application, this study contributes to the growing body of knowledge on CGAs, offering a pathway toward more effective and environmentally conscious technologies.

Acknowledgements This project is funded by the Science Committee of the Ministry of Science and Higher Education of the Republic of Kazakhstan (Grant No. AP19679429).

Author contributions M.Zh. and A.K. wrote the main manuscript text and prepared the figures. M.Zh., Y.A., Y.W., and S.O. contributed to the experimental design, data analysis, and interpretation of the results. M.C., S.C., Y.A., Y.W., and S.O. provided critical revisions to the manuscript. All authors reviewed the final version of the manuscript, approved its claims, and agreed to be authors.

Funding The Science Committee of the Ministry of Science and Higher Education of the Republic of Kazakhstan (Grant No. AP19679429).

Data availability The datasets generated during and/or analysed during the current study are available from the corresponding author on reasonable request.

Declarations

Ethics approval and consent to participate Not applicable.

Consent for publication Not applicable.

Competing interests The authors declare no competing interests.

References

1. Sebba F. Investigations of the Contaminant Capture in CGA (MGD) Foams. USA: 1982.
2. Baigadilov A, Colombano S, Omirbekov S, Cochennec M, Davarzani D, Lion F, Bodiguel H, Oxarango L. Stability and flow behavior of polymer-enhanced foams for improved in-situ remediation of hydrocarbons: Effect of polymer-surfactant interactions. J Hazard Mater. 2025 Mar 15;486:137004. https://doi.org/10.1016/j.jhazmat.2024.137004.
3. Sebba F. Microfoams-an unexploited colloid system. J Colloid Interface Sci. 1971. https://doi.org/10.1016/0021-9797(71)90223-2.
4. Roy D, Valsaraj KT, Constant WD, Darji M. Removal of hazardous oily waste from a soil matrix using surfactants and colloidal gas aphron suspensions under different flow conditions. J Hazard Mater. 1994;38:127–44. https://doi.org/10.1016/0304-3894(94)00028-X.
5. Jauregi P, Mitchell GR, Varley J. Colloidal gas aphrons (CGA): dispersion and structural features. AIChE J. 2000;46:24–36. https://doi.org/10.1002/aic.690460105.
6. Natawijaya MA, Sugai Y, Anggara F. CO2 microbubble colloidal gas aphrons for EOR application: the generation using porous filter, diameter size analysis and gas blocking impact on sweep efficiency. J Pet Explor Prod Technol. 2020;10:103–13. https://doi.org/10.1007/s13202-019-0680-3.
7. Brookey T. "Micro-Bubbles": New Aphron Drill-In Fluid Technique Reduces Formation Damage in Horizontal Wells, 1998.
8. Jauregi P, Varley J. Colloidal gas aphrons: a novel approach to protein recovery. Biotechnol Bioeng. 1998;59:471–81.
9. Hashim M, Mukhopadhyay S, Sen Gupta B, Sahu J. Application of colloidal gas aphrons for pollution remediation. J Chem Technol Biotechnol. 2012. https://doi.org/10.1002/jctb.3691.
10. Sebba F. Polyaphron model for biomembranes. Specul Sci Technol. 1987;10:131–40.
11. Jauregi P, Varley J. Colloidal gas aphrons: Potential applications in biotechnology. Trends Biotechnol. 1999. https://doi.org/10.1016/S0167-7799(99)01363-3.
12. Mansur EHA, Wang Y, Dai Y. Removal of suspensions of fine particles from water by colloidal gas aphrons (CGAs). Sep Purif Technol. 2006. https://doi.org/10.1016/j.seppur.2005.07.022.
13. Matsushita K, Mollah AH, Stuckey DC, del Cerro C, Bailey AI. Predispersed solvent extraction of dilute products using colloidal gas aphrons and colloidal liquid aphrons: aphron preparation, stability and size. Coll Surf. 1992. https://doi.org/10.1016/0166-6622(92)80239-X.
14. Save SV, Pangarkar VG. Characterisation of colloidal gas aphrons. Chem Eng Commun. 1994. https://doi.org/10.1080/00986449408936224.
15. Nareh'ei MA, Shahri MP, Zamani M. Preparation and characterization of colloidal gas aphron based drilling Fluids Usina a Plant-based Surfactant. Society of Petroleum Engineers—SPE Saudi Arabia Section Technical Symposium and Exhibition 2012, 2012. https://doi.org/10.2118/160888-ms.
16. Hosseini SA, Khamehchi E, Dabir B, Alizadeh A, Mansoori Z. Experimental investigation of water based colloidal gas aphron fluid stability. Coll Interfaces. 2019;3:31. https://doi.org/10.3390/colloids3010031.
17. Tabzar A, Arabloo M, Ghazanfari MH. Rheology, stability and filtration characteristics of colloidal gas aphron fluids: role of surfactant and polymer type. J Nat Gas Sci Eng. 2015;26:895–906. https://doi.org/10.1016/j.jngse.2015.07.014.

18. Alamooti A, Colombano S, Omirbekov S, Ahmadi A, Lion F, Davarzani H. Influence of the injection of densified polymer suspension on the efficiency of DNAPL displacement in contaminated saturated soils. J Hazard Mater. 2022. https://doi.org/10.1016/j.jhazmat.2022.129702.
19. Arabloo M, Pordel Shahri M. Experimental studies on stability and viscoplastic modeling of colloidal gas aphron (CGA) based drilling fluids. J Pet Sci Eng. 2014. https://doi.org/10.1016/j.petrol.2013.12.002.
20. Omirbekov S, Colombano S, Alamooti A, Batikh A, Cochennec M, Amanbek Y, et al. Experimental study of DNAPL displacement by a new densified polymer solution and upscaling problems of aqueous polymer flow in porous media. J Contam Hydrol. 2023. https://doi.org/10.1016/j.jconhyd.2022.104120.
21. Abu Elella M, Goda ES, Gab-Allah M, Hong S, Pandit B, Lee S, et al. Xanthan gum-derived materials for applications in environment and eco-friendly materials: a review. J Environ Chem Eng. 2020. https://doi.org/10.1016/j.jece.2020.104702.
22. Sabyrbay B, Davarzani D, Dicharry C, Omirbekov S, Lion F, Alamooti A, Lorthioy M, Krimissa M, Colombano S. Assessment of a novel alcohol-in-biopolymer emulsion for enhanced remediation of diesel-contaminated soils. J Hazard Mater Adv. 2025 Jan 29:100616. https://doi.org/10.1016/j.hazadv.2025.100616.
23. García-Ochoa F, Santos VE, Casas JA, Gómez E. Xanthan gum: Production, recovery, and properties. Biotechnol Adv. 2000. https://doi.org/10.1016/S0734-9750(00)00050-1.
24. Katzbauer B. Properties and applications of xanthan gum. Polym Degrad Stab. 1998;59:81–4. https://doi.org/10.1016/S0141-3910(97)00180-8.
25. Princen HM. Rheology of foams and highly concentrated emulsions: I. Elastic properties and yield stress of a cylindrical model system. J Coll Interface Sci. 1983;91(1):160–75.
26. García-Ochoa F, Santos VE, Casas JA, Gómez E. Xanthan gum: production, recovery, and properties. Biotechnol Adv. 2000;18:549–79. https://doi.org/10.1016/S0734-9750(00)00050-1.
27. Ziaee H, Arabloo M, Ghazanfari MH, Rashtchian D. Herschel-Bulkley rheological parameters of lightweight colloidal gas aphron (CGA) based fluids. Chem Eng Res Des. 2015. https://doi.org/10.1016/j.cherd.2014.03.023.
28. Baigadilov A, Colombano S, Omirbekov S, Cochennec M, Davarzani D, Lion F, et al. Surfactant foam injection for remediation of diesel-contaminated soil: a comprehensive study on the role of co-surfactant in foaming formulation enhancement. Sci Total Environ. 2024;930:172631. https://doi.org/10.1016/J.SCITOTENV.2024.172631.
29. Carullo D, Bosi M, Dermiki M, Bassani A, Jauregi P, Spigno G. Exploring different strategies of separation of antioxidant compounds from winery by-products via surfactant-assisted processes for process intensification and integration. Food Bioprod Process. 2022. https://doi.org/10.1016/j.fbp.2021.11.007.
30. Cho S, Kruger J, van Rooyen A, van Zijl G. Rheology and application of buoyant foam concrete for digital fabrication. Compos B Eng. 2021. https://doi.org/10.1016/j.compositesb.2021.108800.
31. Cho S, van Rooyen A, Kearsley E, van Zijl G. Foam stability of 3D printable foamed concrete. J Build Eng. 2022. https://doi.org/10.1016/j.jobe.2021.103884.
32. Shakeel A, Kirichek A, Chassagne C. Yield stress measurements of mud sediments using different rheological methods and geometries: an evidence of two-step yielding. Mar Geol. 2020. https://doi.org/10.1016/j.margeo.2020.106247.
33. Franco TS, Ellendersen LN, Fattori D, Granato D, Masson ML. Influence of the addition of ovalbumin and emulsifier on the physical properties and stability of yacon (*Smallanthus sonchifolius*) juice foams prepared for foam mat drying process. Food Bioproc Tech. 2015. https://doi.org/10.1007/s11947-015-1553-5.
34. Ahuja A, Lee R, Foster P. Rheology of aqueous foams under pressure. Rheol Acta. 2020. https://doi.org/10.1007/s00397-020-01224-6.
35. Rochinha TN. A study of normal stresses in shear flow of viscoplastic materials. Pontifical Catholic University of Rio de Janeiro, 2021.
36. Binks BP, Kirkland M, Rodrigues JA. Origin of stabilisation of aqueous foams in nanoparticle–surfactant mixtures. Soft Matter. 2008;4:2373–82. https://doi.org/10.1039/B811291F.
37. Khamehchi E, Tabibzadeh S, Alizadeh A. Rheological properties of aphron based drilling fluids. Pet Explor Dev. 2016. https://doi.org/10.1016/S1876-3804(16)30125-2.
38. Spigno G, Amendola D, Dahmoune F, Jauregi P. Colloidal gas aphrons based separation process for the purification and fractionation of natural phenolic extracts. Food Bioprod Process. 2015. https://doi.org/10.1016/j.fbp.2014.06.002.
39. Zhang S, Bao Z, Wu Y, Wang Y, Liu R, Gao Y, et al. Enhancing the stability and effectivity of multiple pesticide formulation mixtures by adding an eco-friendly adjuvant. ACS Sustain Chem Eng. 2023;11:15385–96. https://doi.org/10.1021/acssuschemeng.3c04446.
40. Keshavarzi B, Mahmoudvand M, Javadi A, Bahramian A, Miller R, Eckert K. Salt effects on formation and stability of colloidal gas aphrons produced by anionic and zwitterionic surfactants in xanthan gum solution. 2020. Coll Interfaces. https://doi.org/10.3390/colloids4010009.
41. Le Nguyen Hai N, Sugai Y, Sasaki K. Investigation of stability of CO_2 Microbubbles—colloidal gas aphrons for enhanced oil recovery using definitive screening design. 2020. Coll Interfaces. https://doi.org/10.3390/colloids4020026.
42. Barbosa AM, Santos IJB, Ferreira GMD, da Silva MCH, de Carvalho Teixeira AVN, da Silva LHM. Microcalorimetric and SAXS determination of PEO-SDS interactions: the effect of cosolutes formed by ions. J Phys Chem B. 2014;114(37):11967–74.
43. Ferreira GMD, Ferreira GMD, Agudelo ÁJP, Hespanhol da Silva MC, de Rezende JP, Pires AC, et al. Effect of 1-butyl-3-methylimidazolium halide on the relative stability between sodium dodecyl sulfate micelles and sodium dodecyl sulfate–poly(ethylene oxide) nanoaggregates. J Phys Chem B. 2015;119:15758–68. https://doi.org/10.1021/acs.jpcb.5b09819.
44. Beheshti N, Kjøniksen A-L, Zhu K, Knudsen KD, Nyström B. Viscosification in polymer–surfactant mixtures at low temperatures. J Phys Chem B. 2010;114:6273–80. https://doi.org/10.1021/jp100333f.
45. Fajalia A, Tsianou M. Charging and uncharging a neutral polymer in solution: a small-angle neutron scattering investigation. J Phys Chem B. 2014. https://doi.org/10.1021/jp5023168.
46. Bera A, Ojha K, Mandal A. Synergistic effect of mixed surfactant systems on foam behavior and surface tension. J Surfactants Deterg. 2013. https://doi.org/10.1007/s11743-012-1422-4.
47. Petkova R, Tcholakova S, Denkov ND. Role of polymer–surfactant interactions in foams: effects of pH and surfactant head group for cationic polyvinylamine and anionic surfactants. Coll Surf A Physicochem Eng Asp. 2013;438:174–85. https://doi.org/10.1016/j.colsurfa.2013.01.021.

48. Petkova R, Tcholakova S, Denkov ND. Foaming and foam stability for mixed polymer-surfactant solutions: effects of surfactant type and polymer charge. Langmuir. 2012;28:4996–5009. https://doi.org/10.1021/la3003096.
49. Sadahira MS, Rodrigues MI, Akhtar M, Murray BS, Netto FM. Influence of pH on foaming and rheological properties of aerated high sugar system with egg white protein and hydroxypropylmethylcellulose. LWT. 2018;89:350–7. https://doi.org/10.1016/j.lwt.2017.10.058.
50. Choppe E, Puaud F, Nicolai T, Benyahia L. Rheology of xanthan solutions as a function of temperature, concentration and ionic strength. Carbohydr Polym. 2010. https://doi.org/10.1016/j.carbpol.2010.06.056.
51. Khan SA, Schnepper CA, Armstrong RC. Foam rheology: III. Measurement of shear flow properties. J Rheol. 1988. https://doi.org/10.1122/1.549964.
52. Nareh'ei MA, Shahri MP, Zamani M. Rheological and filtration loss characteristics of colloidal gas aphron based drilling fluids. J Jpn Pet Inst. 2012. https://doi.org/10.1627/jpi.55.182.
53. Ferry JD. Viscoelastic properties of polymers. Hoboken: Wiley; 1980.
54. Marze S, Guillermic RM, Saint-Jalmes A. Oscillatory rheology of aqueous foams: surfactant, liquid fraction, experimental protocol and aging effects. Soft Matter. 2009. https://doi.org/10.1039/b817543h.
55. Mason TG, Bibette J, Weitz DA. Elasticity of compressed emulsions. Phys Rev Lett. 1995. https://doi.org/10.1103/PhysRevLett.75.2051.
56. Rouyer F, Cohen-Addad S, Höhler R. Is the yield stress of aqueous foam a well-defined quantity? Coll Surf A Physicochem Eng Asp. 2005. https://doi.org/10.1016/j.colsurfa.2005.01.025.
57. Stevenson P. Foam engineering: fundamentals and applications. Hoboken: Wiley; 2012.
58. Dang MT, Denisov D, Struth B, Zaccone A, Schall P. Reversibility and hysteresis of the sharp yielding transition of a colloidal glass under oscillatory shear. Eur Phys J E. 2016;39:44. https://doi.org/10.1140/epje/i2016-16044-3.
59. Moghimi E, Jacob AR, Koumakis N, Petekidis G. Colloidal gels tuned by oscillatory shear. Soft Matter. 2017;13(12):2371–83. https://doi.org/10.1039/C6SM02508K.
60. Park JD, Ahn K, Lee S. Structural change and dynamics of colloidal gels under oscillatory shear flow. Soft Matter. 2015. https://doi.org/10.1039/c5sm01651g.
61. Vaart K, Rahmani Y, Zargar R, Bonn D, Schall P. Rheology of concentrated soft and hard-sphere suspensions. J Rheol. 2013;57:1195. https://doi.org/10.1122/1.4808054.
62. Martikainen L, Bertula K, Turunen M, Ikkala O. Strain stiffening and negative normal force of agarose hydrogels. Macromolecules. 2020;53:9983–92. https://doi.org/10.1021/acs.macromol.0c00601.